

Rheology of Polydisperse non-Spherical Graphite Particles Suspended in Mineral Oil

Larsen, Thomas; Søbbye, A. L.; Royer, J. R.; Poon, W. C. K.; Larsen, Tom; Andreasen, S. J.; Drozdov, A. D.; Christiansen, J. D. C.

DOI (link to publication from Publisher):
[10.48550/arXiv.2207.02720](https://doi.org/10.48550/arXiv.2207.02720)

Publication date:
2022

Document Version
Early version, also known as pre-print

[Link to publication from Aalborg University](#)

Citation for published version (APA):
Larsen, T., Søbbye, A. L., Royer, J. R., Poon, W. C. K., Larsen, T., Andreasen, S. J., Drozdov, A. D., & Christiansen, J. D. C. (2022). *Rheology of Polydisperse non-Spherical Graphite Particles Suspended in Mineral Oil*. arXiv. <https://doi.org/10.48550/arXiv.2207.02720>

General rights

Copyright and moral rights for the publications made accessible in the public portal are retained by the authors and/or other copyright owners and it is a condition of accessing publications that users recognise and abide by the legal requirements associated with these rights.

- Users may download and print one copy of any publication from the public portal for the purpose of private study or research.
- You may not further distribute the material or use it for any profit-making activity or commercial gain
- You may freely distribute the URL identifying the publication in the public portal -

Take down policy

If you believe that this document breaches copyright please contact us at vbn@aub.aau.dk providing details, and we will remove access to the work immediately and investigate your claim.

Rheology of Polydisperse non-Spherical Graphite Particles Suspended in Mineral Oil

Th. Larsen,^{1,2} A. L. Sørensen,^{1,2} J. R. Royer,³ W. C. K. Poon,³ T. Larsen,² S. J. Andreasen,² A. D. Drozdov,¹ and J. D. C. Christiansen^{1, a)}

¹⁾*Department of Materials and Production, Aalborg University, 9000 Aalborg, Denmark*

²⁾*Advent Technologies A/S, 9000 Aalborg, Denmark*

³⁾*School of Physics and Astronomy, University of Edinburgh, Edinburgh EH9 3FD, United Kingdom*

(Dated: 7 July 2022)

We study the role of filler concentration and microphysics on the rheology of polydisperse flake-graphite particles suspended in Newtonian mineral oil. Under steady shear, shear thinning becomes more pronounced when shearing from low to high rates than in the opposite direction. We attribute this to a greater degree of filler orientation during up-shear. Time-temperature superposition was observed using an Arrhenius-type horizontal shift factor, giving a flow activation energy that is dependent on the graphite volume fraction, suggesting concentration-dependent contributions to relaxation processes in the suspensions. The flow curves are fitted by a constraint-based model, indicating that the flow behaviour is controlled by frictional and adhesive contacts, with the model suggesting that the adhesive stress is temperature dependent.

I. INTRODUCTION

Carbonic polymer composites are widely applicable, for instance as electrode materials in fuel cell bipolar plates (BPPs), as porous electrodes in Li-ion batteries, or in aerospace composites, and hence, their properties have been intensively studied¹⁻⁷. In BPP applications, replacing traditional materials such as graphite with highly-filled carbonic polymer composites can give higher electrical and thermal conductivities at relatively low costs⁸. The high filler loadings required to obtain satisfactory conductivities may, however, dramatically affect the composite rheology^{9,10}, hereby complicating manufacturing. Yet, characterising the rheological properties of carbonic polymer composites may yield valuable insight into the microstructure, filler dispersion and filler interactions since this information correlates with electrical properties¹¹. Thus, rational composite design requires understanding how the filler particles, the matrix phase and their coupling affect the system's rheology. Additionally, the importance of understanding the coupling between phases extends to e.g. semi-solid flow cells where the flowing electrodes consist of suspensions of active (LiFePO₄) and conductive (carbon black) materials. Tuning particle interactions in such biphasic mixtures allows control of their rheology and hence reduction of particle sedimentation and phase segregation, as well as enabling efficient charge transport¹².

The matrix in graphite-polymer composites is typically a thermoplastic such as poly(methyl-methacrylate), polyethylene, polyvinyl chloride, etc., and their derivatives. The rheology of their melts at processing temperatures is by now well understood^{13,14}. This provides a good starting point for the predictive formulation of the matrix component of graphite-polymer composites.

The filler, graphite, can be exfoliated into colloidal flakes^{15,16}. However, most commercial graphite powder ad-

ditives fall in the non-Brownian regime, with typical particle size $\gtrsim 10\mu\text{m}$. Compared to polymer melts, the rheology of non-Brownian suspensions is poorly understood. Such systems are history-dependent because no thermal motion randomises particle positions. Moreover, it has recently become clear that particle contacts control rheology¹⁷, and contact forces are far more sensitive to surface details, e.g., hydrogen bonding¹⁸, than non-contact colloidal interactions. Many uncertainties therefore remain, with experimental validation of simulations¹⁹ and theory²⁰ largely limited to model non-Brownian suspensions of nearly-monodispersed repulsive spheres²¹⁻²³, although results for the role of adhesive contact interactions are now beginning to emerge²⁴⁻²⁶. Not surprisingly, then, highly non-intuitive discoveries are still being made, such as bistability in non-Brownian particles dispersed in a colloidal gel matrix²⁷.

Current knowledge therefore does not yet constitute a firm basis for the predictive formulation of graphite-polymer composite fillers. In this work, we contribute towards this goal by studying a model composite in which the non-Newtonian polymer melt matrix at processing temperatures is replaced by a simpler Newtonian fluid. We then probe whether the recently-emergent framework of 'contact-force rheology'^{17,24} may be applicable to one popular form of graphitic particles.

Specifically, we explore the rheology of polydisperse graphite particles dispersed in mineral oil using rotational rheometry, varying the solid volume fraction, ϕ , and temperature, T . A weak flow-history dependence may be attributable to filler orientation. We re-scale flow curves from different T , and fit these with the purely empirical Herschel-Bulkley model and a recent physics-based model. The latter approach allows us to infer mechanistic insights concerning adhesive and frictional inter-particle contacts. As background, we first review briefly the new framework of suspension rheology involving inter-particle contacts.

^{a)} Author to whom correspondence should be addressed; electronic mail: jc@mp.aau.dk

II. CONTACT FORCES IN SUSPENSION RHEOLOGY

Developing constitutive models for non-Brownian, or granular, suspensions is a longstanding challenge²⁸. Recent advances have identified an essential piece of missing physics. Simulations¹⁹ and theory²⁰ suggest that at high enough applied stress, particles are pressed into frictional contact. This effect is included in a simple model²⁰ that starts from the well-known phenomenological equation^{29–31}

$$\eta_r = \left(1 - \frac{\phi}{\phi_J}\right)^{-l}, \quad (1)$$

with $\eta_r = \eta/\eta_0$ the suspension viscosity, η , relative to that of the suspending solvent, η_0 , and the exponent³² $l \approx 2$. This so-called Krieger-Dougherty equation captures the well-known observation that the viscosity of any suspension will diverge when its volume fraction, ϕ , reaches some ‘jamming’ point ϕ_J . In the original formulation, ϕ_J is a constant for any particular suspension. Subsequently, it has been suggested that ϕ_J is shear-rate dependent^{33,34}. The recent breakthrough comes from the realisation that ϕ_J is in fact dependent on the applied stress, σ , for which Wyart and Cates (WC) propose the form

$$\phi_J(\sigma) = \phi_{\text{rlp}} f(\sigma) + \phi_{\text{rcp}} [1 - f(\sigma)]. \quad (2)$$

This is a linear interpolation between random close packing, ϕ_{rcp} in the low-stress limit and random loose packing, $\phi_{\text{rlp}} < \phi_{\text{rcp}}$, in the high-stress limit. The crucial physics idea is that as the applied stress increases, an increasing fraction f of particles are pressed into frictional contact. The no-sliding constraint imposed by static friction then dictates a looser form of packing, so that as f increases from 0 to 1, the jamming point ϕ_J decreases from random close packing to random loose packing, with the latter being dependent on the coefficient of static friction, μ , between the particles. For non-frictional hard spheres, $\phi_{\text{rcp}} \approx 0.64$, and $\phi_{\text{rlp}} \approx 0.55$ in the high friction limit ($\mu \gtrsim 1$)³⁵. WC propose that the transition between these two packing limits occurs at some characteristic ‘onset stress’ σ^* for frictional contact. Any form of $f(\sigma)$ that increases with σ predicts shear thickening when Equation 2 is substituted into Equation 1: η_r increases as σ increases because ϕ_J decreases with σ . A sigmoidal $f(\sigma)$ captures the measured rheology of a variety of shear thickening systems with only a handful of fitting parameters^{21–23}.

This framework can be extended to include adhesive contacts that constrain rolling, which are released under increasing stress²⁴. Such rolling constraints, which could arise between attractive particles due to contact pinning or touching facets, introduce a new critical packing fraction, ‘adhesive loose packing’, $\phi_{\text{alp}} < \phi_{\text{rlp}}$. This limit is not precisely known even for monodisperse spheres, although simulations³⁶ suggest that it could be as low as $\phi_{\text{alp}} \approx 0.14$. Analogous to $f(\sigma)$, a function $a(\sigma)$ describes the release of these constraints by applied stress, with $a(\sigma \rightarrow 0) = 1$ and $a(\sigma \rightarrow \infty) = 0$. The extended WC model including such adhesive contacts predicts a ‘zoo’ of flow curves involving combinations of shear thinning and shear thickening²⁴.

In the limit where contacts are always frictional³⁷, i.e. $f = 1$ at all σ , we write

$$\phi_J(\sigma) = \phi_{\text{alp}} a(\sigma) + \phi_{\text{rlp}} [1 - a(\sigma)]. \quad (3)$$

An inverse sigmoidal form

$$a(\sigma) = 1 - \exp\left[-(\sigma_a/\sigma)^\beta\right] \quad (4)$$

is able to capture the rheology of a variety of systems, including PMMA spheres in oil²⁴, cornstarch in oil²⁵, calcite in glycerol-water²⁶ and molten chocolate (= sugar grains in oil)³⁸. In Equation 4, σ_a gives a characteristic stress scale for peeling adhesive contacts apart to initiate rolling, while β describes the rate $a(\sigma)$ decreases from 1 to 0. Importantly, a finite yield stress, $\sigma_y > 0$, is predicted at $\phi > \phi_{\text{alp}}$. At and below this stress, the viscosity diverges in the flow curve. Solving $\eta^{-1}(\sigma) = 0$ using the above ansatz for $a(\sigma)$ gives

$$\sigma_y(\phi) = \sigma_a \left[\ln \left(\frac{\phi_{\text{rlp}} - \phi_{\text{alp}}}{\phi - \phi_{\text{alp}}} \right) \right]^{-1/\beta}, \quad (5)$$

which describes $\sigma_y(\phi)$ data in calcite suspensions²⁶. Note that the yield stress involves the cooperative action of adhesion *and* friction²⁵, with adhesive contacts stabilising frictional force chains. Moreover, Equation 5 predicts $\sigma_y \rightarrow \infty$ at ϕ_{rlp} , just as in purely frictional systems: irrespective of adhesion, friction prevents flow above random loose packing.

In this model, many effects enter through the values of ϕ_{alp} and ϕ_{rlp} . In particular, their values depend on particle shape and polydispersity: irregular particles jam at lower volume fractions compared to spheres³⁹ while polydispersity enables denser packing⁴⁰. Moreover, this simple model will not account for effects such as shear-induced alignment of anisotropic particles. Nevertheless, we will find fitting this model to our graphite-in-oil data gives significant insight into the physical factors controlling the rheology of this system.

III. MATERIALS AND METHODS

Timcal Timrex KS5-75TT graphite particles with a size distribution of $D_{10} = 9.1 \mu\text{m}$, $D_{50} = 38.8 \mu\text{m}$, and $D_{90} = 70.0 \mu\text{m}$ (supplier’s laser diffraction data) were obtained from Imerys Graphite & Carbon. They have a Scott density of 0.44 g cm^{-3} and a tapped density of 2.2 g cm^{-3} , and are predominately flake-like with an irregular surface. However, included are also more oblate- and needle-shaped particles, Figure 1. Suspensions at different volume fractions, ($\phi = 0.10, 0.15, 0.18, 0.20, 0.23, 0.25, 0.27, 0.28, 0.29$), were prepared by mechanically mixing heavy mineral oil (Merck 330760; viscosity $\eta_0 = 0.14 \text{ Pas}$ at 25°C) with graphite powder. In between experiments the suspensions were stored at room temperature.

For rheological measurements an AR-G2 rheometer (TA Instruments) was used, and temperature (10°C to 35°C) was controlled with a Peltier system. A parallel plate geometry (diameter 40 mm , gap height $600\text{--}1000 \mu\text{m}$) with cross-hatching was used to obtain data for suspensions, while for



FIG. 1. Scanning electron microscopy image of the Timcal Timrex KS5-75TT graphite particles used in this study obtained using a Zeiss EVO LS15 with an EHT of 10kV.

the pure oil a smooth parallel plate geometry (same diameter, gap height 500 μm) was used. Suspensions were mechanically homogenised prior to loading. Samples at $\phi < 0.27$ were pre-sheared for 30 s at a shear rate $\dot{\gamma} = 10 \text{ s}^{-1}$ to erase memory of the loading history. At $\phi \geq 0.27$ we pre-sheared for 30 s at $\sigma = 150 \text{ Pa}$ or $\dot{\gamma} = 0.5 \text{ s}^{-1}$ to avoid edge fracture. All samples equilibrated to the measurement temperature for 3 min before starting the experiment. Steady shear measurements were performed on the $\phi = 0.10, 0.15, 0.18, 0.20, 0.23, 0.25$ suspensions to study time-temperature superposition, with gap heights of 600, 800, and 1000 μm at each temperature to check that wall slip effects were insignificant^{12,38,41}. Unless explicitly stated, we sheared from low to high rates, and report flow curves that are the average of at least two measurements.

Brownian motion and inertia effects can be neglected because $\text{Pe} \gg 1$ and $\text{Re} < 10^{-3}$ throughout our range of $\dot{\gamma}$. The minimum stress required for counteracting sedimentation is estimated as $\sigma_{\min} = \Delta\rho g D^{25,26}$, where $\Delta\rho$ is the particle fluid density difference, g is the acceleration of gravity, giving $\sigma_{\min} \approx 0.5 \text{ Pa}$ using $D = D_{50}$. This is similar to the lowest measured stresses in the two least concentrated suspensions, so that we may also neglect sedimentation effects.

IV. RESULTS AND DISCUSSION

A. Influence of sweep direction

Rotational shear rheometry data for suspensions of $\phi = 0.15, \phi = 0.20$, and 0.25 sweeping from high \rightarrow low (HL) and low \rightarrow high (LH) shear rates are shown in Figure 2a. Each sample was only swept in one direction to probe the effect of sweep direction. All samples exhibit sweep direction-dependent shear thinning. Furthermore, the low-shear viscosities show increasing relative deviation with graphite concentration.

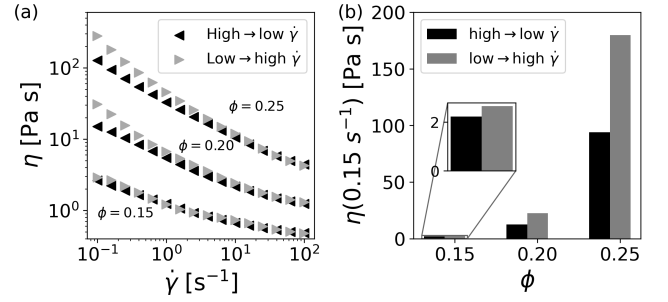


FIG. 2. (a) Steady shear viscosity (η) at 25 $^{\circ}\text{C}$ as a function of shear rate ($\dot{\gamma}$) for suspensions at $\phi = 0.15, \phi = 0.20$, and $\phi = 0.25$ measured by rotational rheometry without pre-shearing, sweeping from high \rightarrow low and low \rightarrow high shear rate using a new sample for each direction. Data are based on single samples. (b) Viscosities measured at $\dot{\gamma} = 0.15 \text{ s}^{-1}$. The relative viscosity difference between low \rightarrow high and high \rightarrow low sweeps at $\dot{\gamma} = 0.15 \text{ s}^{-1}$ are 19 % ($\phi = 0.15$), 79 % ($\phi = 0.20$), and 92 % ($\phi = 0.25$).

The dependence on the sweep direction may reflect shear-induced changes in the suspension microstructure. Such shear-induced orientational alignment at high $\dot{\gamma}$ has been observed in aqueous suspensions of cellulose microcrystals⁴² and platelet-like organoclays in polypropylene/organoclay nanocomposites⁴³. Shear thinning in suspensions of non-Brownian spheres can also be associated with breakdown of large agglomerates under increasing shear⁴⁴. This suggests a picture where our flake-like graphite particles initially exist as irregular clusters after loading, so that sweeping from high \rightarrow low $\dot{\gamma}$ can break apart the clusters into flakes which then orient under shear, resulting in a lower viscosity at low shear rates. In contrast, sweeping in the opposite direction from low \rightarrow high $\dot{\gamma}$ would largely preserve these irregular clusters at low rates and avoid significant alignment. In this scenario, we would expect the magnitude of this viscosity difference to increase with the filler concentration, as the irregular clustered state should have a lower jamming density than the aligned state, consistent with our observations, Figure 2b. Particle alignment will likely be most severe in the uniform linear shear applied in rotational rheometry, while practical mixing processes tend to feature non-uniform flows that will inhibit alignment. We therefore focus on the flow curves obtained from low \rightarrow high shear rate sweeps in the remaining sections of this work.

B. Temperature dependence

The flow curves of selected suspensions with $\phi \leq 0.25$ at 10 $^{\circ}\text{C}$ to 35 $^{\circ}\text{C}$ are shown in Figure 3a. A common approach to analysing temperature-dependent rheology is time-temperature superposition (TTS), where (typically) the shear rates are shifted by some temperature-dependent factors a_T to align the flow curves to that measured at some reference temperature. We shift our flow curves $\sigma(\dot{\gamma}, T)$ by the scaling $\dot{\gamma} \rightarrow a_T \dot{\gamma}$, Figure 3b, to arrive at a set of concentration-dependent shift factors $a_T(\phi)$, Figure 4a. These follow an

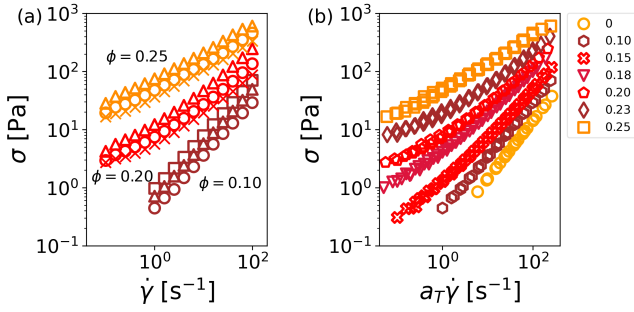


FIG. 3. (a) Stress (σ) as a function of shear rate ($\dot{\gamma}$) at $T = 10$ °C (\square), 15 °C (\triangle), 25 °C (\circ) and 35 °C (\times). (b) Time-temperature superposition of stress as a function of shifted shear rate ($a_T \dot{\gamma}$) at a reference temperature of 25 °C.

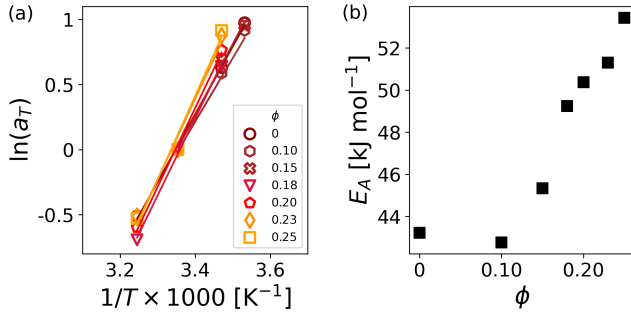


FIG. 4. (a) Shift factors (a_T), used for time-temperature superposition of the data in Figure 3b, as a function of inverse temperature ($1/T$). The natural logarithm of the shift factors follow an Arrhenius-dependence (solid lines), Equation 6. (b) Flow activation energies E_A as a function of graphite volume fraction ϕ , calculated from the Arrhenius-model fits in (a). E_A exhibits a dependence on the graphite volume fraction.

Arrhenius-type dependence,

$$\ln a_T(\phi) = \frac{E_a(\phi)}{R} \left(\frac{1}{T} - \frac{1}{T_{\text{ref}}} \right), \quad (6)$$

where E_a is the flow activation energy, R the universal gas constant, and $T_{\text{ref}} = 25$ °C the reference temperature. Plotting $E_a(\phi)$, Figure 4b, reveals a rapid increase at $0.15 \lesssim \phi \lesssim 0.20$. Interestingly, $\phi = 0.20$ is the first concentration at which we may discern a flattening at low σ in the flow curve as ϕ increases, Figure 3b, and therefore the emergence of a finite yield stress.

TTS has been applied to a variety of non-Brownian suspensions, including silica in ethylene glycol/glycerol with added salt⁴⁵, glass spheres in polyisobutylenes⁴⁶ and PMMA spheres (diameter $> 1 \mu\text{m}$) in poly(ϵ -caprolactone)⁴⁷. In these cases with Newtonian solvents, the suspended solids do not significantly affect the relaxation dynamics and hence shift factors. In cases where the matrix is non-Newtonian, there is more variation from system to system, with little to no change with filler concentration in glass fiber reinforced polypropylene⁴⁸ or Newtonian epoxy resin filled with multi-walled carbon nanotubes (MWCNTs)⁴¹, while the activation

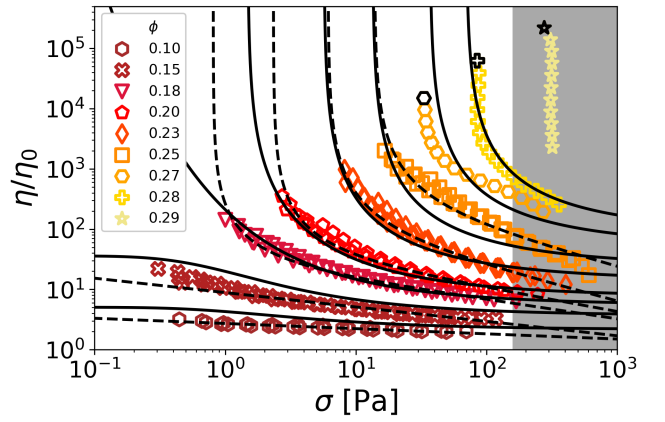


FIG. 5. The relative viscosity (η/η_0) at 25 °C as a function of shear stress (σ) at various ϕ . The dashed lines show Herschel-Bulkley model fits, Equation 8, with parameters shown in Figure 6. The solid lines are the fits to the constraint-based model, Equation 1, Equation 3 and Equation 4, with $l = 2$, $\sigma_a = 5.4$ Pa, $\beta = 0.49$, $\phi_{\text{lp}} = 0.31$ and $\phi_{\text{alp}} = 0.18$. Shaded area marks the region of sample fracture where the data are excluded from our fitting.

energy was found to increase with concentration in nitrile-butadiene/graphene nanocomposites⁴⁹ and decrease with concentration in MWCNT/polycarbonate composites⁵⁰.

We will later apply the adhesive constraints model reviewed earlier to our system, which assumes a purely stress-dependent rheology, i.e., $\eta(\sigma) = \eta_0 \mathcal{F}(\phi, \sigma)$ for some function $\mathcal{F}(\phi, \sigma)$. In this case, we have

$$\frac{\sigma}{\eta_0(T) \dot{\gamma}} = \mathcal{F}(\phi, \sigma) = \frac{\sigma}{\eta_0(T_{\text{ref}}) a_T \dot{\gamma}} \Rightarrow a_T = \eta_0(T) / \eta_0(T_{\text{ref}}), \quad (7)$$

which we recognise as the shift factor for the pure solvent. So, we predict a ϕ -independent suspension shift factor, as was observed in many previous systems^{45–47}. Figure 4b therefore suggests an additional source of temperature-dependence beyond the solvent in our graphite-in-oil suspensions.

C. Phenomenological fitting

Figure 3b suggests that a finite yield stress emerges at $\phi \gtrsim 0.20$. Flow curves for yield-stress fluids are often fitted empirically by the Herschel-Bulkley (HB) equation^{51,52}

$$\sigma = \sigma_y + K \dot{\gamma}^n, \quad (8)$$

where σ_y is the HB yield stress, K the consistency index, and n the flow index ($n > 1$ for shear thickening, $n < 1$ for shear thinning). This equation, which fits data from disparate systems from colloidal gels and glasses through jammed emulsions⁵³ to certain non-Brownian suspensions^{29,44}, also credibly applies to our data for $\phi \leq 0.25$, Figure 5.

The fitted HB yield stress σ_y is plotted as a function of ϕ in Figure 6a, where we have assigned $\sigma_y = 0$ to all systems with $\phi \leq 0.15$. This reflects the lack of a low- σ plateau in the relevant flow curves, Figure 3, and is consistent with our

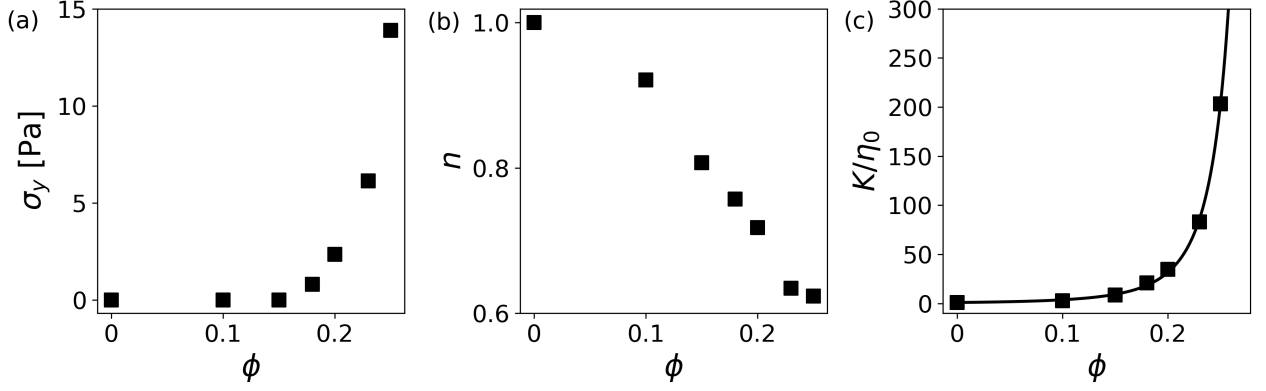


FIG. 6. Parameters from the Herschel-Bulkley fit to the time-temperature superposition data, Figure 5, as a function of the graphite volume fraction ϕ . (a) Yield stress, σ_y . (b) Flow index, n . (c) Normalized consistency index, K/η_0 , with the Krieger-Dougherty model (solid line) from Equation 1 fitted to the data using $l_{KD} = 3.55$ and $\phi_{J,KD} = 0.32$.

experience of handling these samples, which flowed easily as liquids. The extracted HB yield stress increases rapidly for $\phi \gtrsim 0.20$, Figure 6a, suggesting a divergence at some critical concentration.

The flow index n steadily decreases with increasing graphite volume fraction, Figure 6b, from $n = 1$ for our Newtonian mineral oil ($\phi = 0$) to $n \approx 0.6$ for $\phi = 0.25$, indicating an increasing degree of shear thinning. This contrasts with yield stress suspensions of spherical particles, where the ϕ dependence is either weaker²⁹ or absent⁴⁴. Our observation possibly reflects a particle shape effect.

Like σ_y , the consistency index K also increases with ϕ and appears to diverge, Figure 6c. The data can be fitted to $K \propto (1 - \phi/\phi_{J,KD})^{-l_{KD}}$ with $\phi_{J,KD} = 0.32$ and $l_{KD} = 3.55$ (KD = Krieger-Dougherty). The consistency index scales as the viscosity at $\dot{\gamma} = 1 \text{ s}^{-1}$ and it may be interpreted as a kind of ‘generalised viscosity’. Perhaps unsurprisingly, $\phi_{J,KD}$ will be related to a viscosity divergence to be identified later.

D. Physical modelling

The HB equation is purely phenomenological and contains no physics. In contrast, a recently-proposed constraint-based model²⁴ is predicated on the existence of adhesive and frictional contacts. Fitting to this model may therefore yield insights into the micro-physics of our graphite suspensions.

Since our flow curves all show shear thinning ($d\eta_r/d\sigma < 0$) without subsequent shear thickening, Figure 5, we apply the model in the limit where particle contacts are frictional at all stresses ($f = 1$). Adhesive constraints to rolling that are progressively released as stress increases give rise to yielding and subsequent shear thinning. This is similar to suspensions of cornstarch in oil²⁵ and unstabilised calcite in glycerol-water²⁶.

The model, which, has been reviewed above, requires five parameters: l the viscosity divergence exponent, two critical volume fractions ϕ_{rlp} and ϕ_{alp} reflecting the frictional and

frictional+adhesive jamming points, and the stress scale σ_a and exponent β describing the release of adhesive constraints. If particle contacts do not change with ϕ , a single set of ϕ -independent parameters should fit all our flow curves. This is in contrast to the HB fits, with either two or three free parameters per flow curve.

Sample fracture was observed at $\sigma > 160 \text{ Pa}$, so that the data in the shaded region in Figure 5 are not used for fitting. Fitting to the rest of the data gives $\sigma_a = 5.4 \text{ Pa}$ for the release of adhesive rolling constraints, with an exponent $\beta = 0.49$. The latter is in line with previous work that found $0.5 \lesssim \beta \lesssim 0.6$ ^{24,26}, evidencing a similar rate of release of rolling constraints.

Our fitted value of $\phi_{rlp} = 0.31$ is close to $\phi_{J,KD} = 0.32$ obtained from the consistency index data from fitting to the KD equation, Figure 6c. This concentration is where friction alone suffices to cause jamming, and is well below the random loose packing limit for monodisperse frictional spheres, even in the limit of infinite static friction, where $\phi_{rlp} \approx 0.55$ ³⁵. Interestingly, this latter value appears not particularly dramatically sensitive to details of particle morphology, as fitting the same model to suspensions of more or less isotropic calcite crystals also returns $\phi_{rlp} \approx 0.55$ ²⁶. However, gross changes in morphology do have an effect. Fitting $K(\phi)$ in suspensions of prolate wollastonite with a mean aspect ratio of 9 suspended in silicone oil returned $\phi_{rlp} = 0.32$ - 0.34 ²⁹, which is close to the value for our suspensions of oblate and needle-shaped graphite particles. While polydispersity will increase ϕ_{rlp} ^{13,40}, in our case, the non-spherical particle morphology apparently completely counteracts this effect.

Equation 5 is one of the key predictions of the adhesive constraint model. It shows that a finite yield stress should only emerge at ϕ_{alp} ; thereafter, σ_y increases until it diverges at ϕ_{rlp} . To test this prediction, we collected flow curves at three additional higher volume fractions, $\phi = 0.27, 0.28$ and 0.29 , Figure 5, to obtain $\sigma_y(\phi)$ over as wide a range of ϕ as possible. The yield stresses for these three flow curves were obtained by eye as the highest stress value reached in each

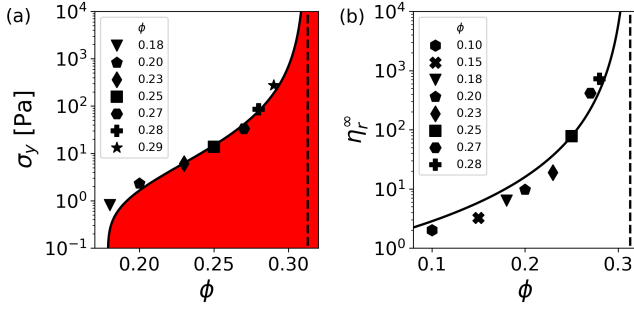


FIG. 7. (a) Yield stresses (σ_y) from Figure 6a, including $\sigma_y(\phi = 0.27) = 33.2$ Pa, $\sigma_y(\phi = 0.28) = 84.9$ Pa, and $\sigma_y(\phi = 0.29) = 277$ Pa (black symbols in Figure 5) measured at the lowest shear rate. Data are consistent with predictions by Equation 5 (solid line) using the parameters found by fitting the flow curves in Figure 5. Shaded (red), jammed; unshaded, flowing. Dotted line, $\phi_{rlp} = 0.31$. (b) Relative viscosity values before fracture (η_r^∞) fitted to $\eta_r^\infty = (1 - \phi/\phi_{rlp})^{-l}$ using $l = 2.72$ and $\phi_{rlp} = 0.31$ (dotted vertical line).

case (sometimes called the ‘apparent yield stress’⁵⁴). These three yield stresses are plotted together with those obtained by fitting the HB equation in Figure 7a. Equation 5 (the full line) with the constraint-model parameters from Figure 5 is seen to be consistent with this data. Below $\phi_{alp} \approx 0.18$, adhesive contacts are insufficient to stabilise frictional force chains²⁵ so that a non-flowing state never forms – there is no yield stress. At $\phi_{rcp} \approx 0.31$, frictional force chains are stable irrespective of adhesion, and the system is permanently jammed. The latter is also evidenced by a plot of the high-shear viscosity against volume fraction, Figure 7b, which shows a divergence at a concentration that is consistent with ϕ_{rlp} .

It is intriguing that our fitted value of $\phi_{alp} \approx 0.18$ is comparable to that found for suspended particles of adhesive calcite²⁶ and PMMA²⁴ (≈ 0.18 and 0.20 respectively) even though our fitted value of $\phi_{rlp} \approx 0.31$ is considerably below the value of ≈ 0.55 obtained for these two systems. Intuitively, one may expect adhesive loose packing to correlate with contact percolation. Particle clusters in sheared non-colloidal suspensions may form a percolated network around a volume fraction of $0.3 - 0.4$ for monodisperse spheres⁵⁵, with lower thresholds for anisotropic particles. So, carbon nanotubes may percolate at as low as $0.3-0.8$ wt.% in polycarbonate⁵⁰, corresponding to $\phi \lesssim 0.005$. Similarly, the electrical percolation threshold of polymer composites decreases with filler aspect ratio⁵⁶. We may therefore expect ϕ_{alp} for our flake-like graphite particles to be lower, if not significantly lower, than that in adhesive PMMA spheres²⁴ or calcite crystals that do not show gross geometric anisotropy²⁶. These considerations suggest that contact percolation alone is insufficient for adhesive loose packing. This is expected from the physical picture associated with the adhesive constraint model²⁶, that ϕ_{alp} is the lowest concentration at which adhesive contacts can stabilise frictional force chains to cause jamming. In other words, these contacts do *not* act alone, so that percolation *per se* is insufficient, explaining the observation that the fitted

$\phi_{alp} \approx 0.18$ in our graphite suspensions is considerably higher than what one may expect to be needed for contact percolation alone.

Finally, we return to the unexpected temperature-dependent flow behaviour, which manifested as a sharp increase in the TTS shift factors above $\phi = 0.15$, Figure 4b. Plotting the relative viscosities $\eta/\eta_0(T)$ at 15°C , 25°C and 35°C against the shear stress, we see that data collapse becomes progressively worse as ϕ increases, and becomes very noticeable for $\phi > 0.15$, Figure 8a. However, we find that shifting the *stress* by a temperature-dependent factor, $a_\sigma(T)$, improves the data collapse noticeably, especially at $\phi \geq 0.15$, Figure 8b. Fitting the resulting flow curves to the adhesive constraint model, Figure 8c, using a fixed β -value, $\phi_{rlp} = 0.31$ and $\phi_{alp} = 0.18$ then suggests a temperature-dependent characteristic adhesive stress $\sigma_a = \sigma_a(T)$, which, as expected, is anti-correlated with the temperature-dependent shift factor $a_\sigma(T)$, Figure 8d.

The finding that σ_a decreases with temperature suggests rolling constraints are more easily released at higher temperatures. The origin of this effect in our system is currently unobvious. The van der Waals interaction should be temperature-independent in our temperature range⁵⁷, so that there is another source of rolling constraint that is more specific to our graphite suspensions. It would be fruitful to examine whether solvent-mediated interactions, such as improved wetting driven by a decreased oil surface tension with temperature could be the source of this temperature dependence. Whatever its source, a temperature-dependent σ_a provides a handle for controlling the rheology of our system. (Note that such temperature variation in σ_a does not change the critical packing limits in Equation 5, only the relative magnitude of the yield stress.)

V. CONCLUSION

Polydisperse flake-like graphite particles suspended in heavy mineral oil were investigated using rotational rheometry. Sweeping high \rightarrow low shear rates resulted in lower viscosities at low shear rates than sweeping low \rightarrow high. We suggest that this is because the graphite particles are initially in a clustered state, which breaks down at high shear rates and causes orientation of fillers in the flow. Time-temperature superposition of the flow curves revealed an Arrhenius-type dependence of the horizontal shift factors with an increasing flow activation energy with filler concentration above a threshold graphite volume fraction $\phi \approx 0.15$.

We were able to account for our observations by fitting to a recent constraint-based model of non-Brownian suspension rheology²⁵ in which frictional and adhesive contacts constrain sliding and rolling motion, respectively. Above a critical concentration ϕ_{alp} , adhesive stabilisation of frictional force chains gives rise to a finite yield stress, which diverges at a higher ϕ_{rlp} , at which frictional contacts alone suffice for mechanical stability. At all $\phi < \phi_{rlp}$, stress-induced release of adhesive rolling constraints causes shear thinning, allowing particles to align themselves in the flow direction.

Our analysis suggests a temperature-dependent characteris-

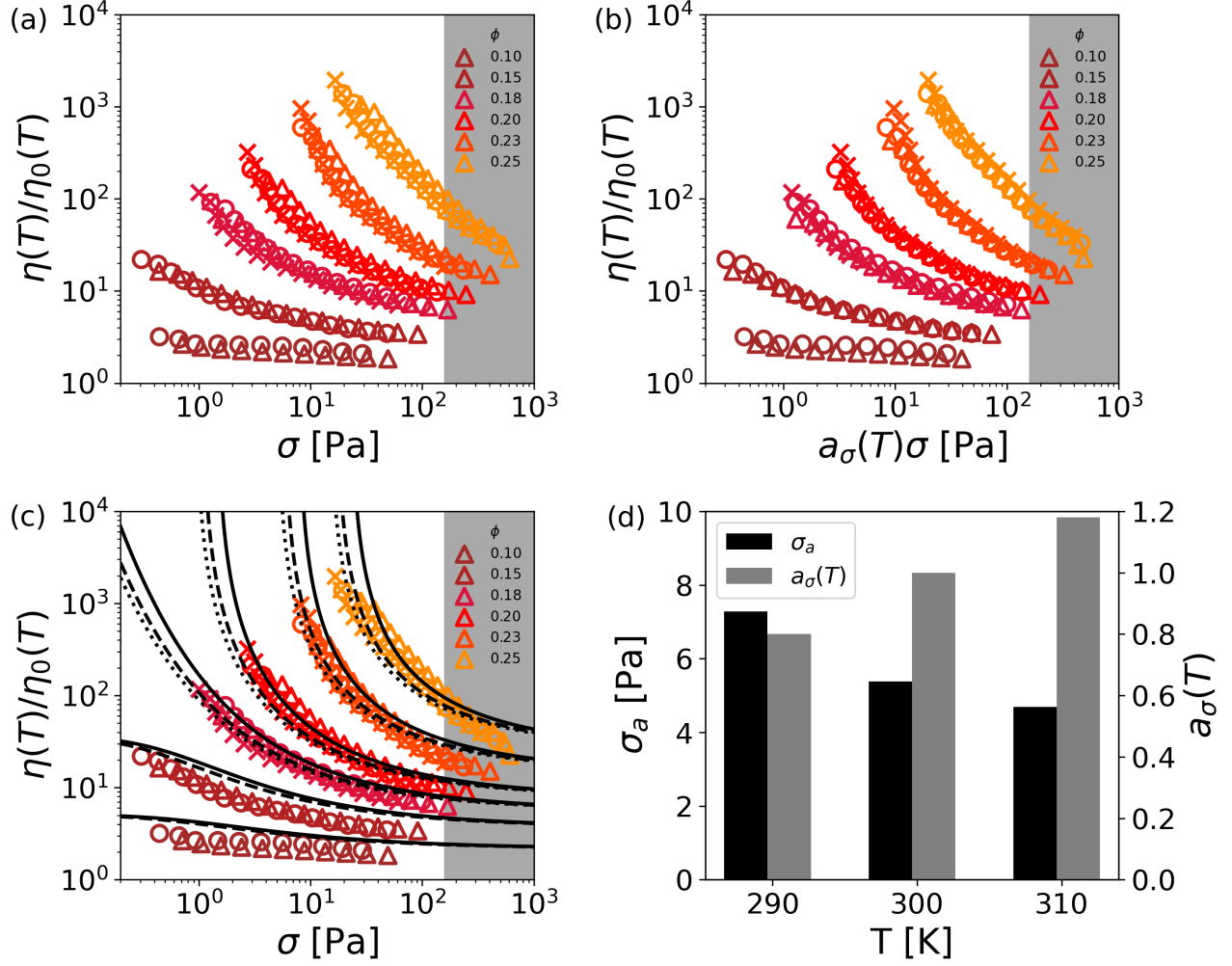


FIG. 8. (a) Relative viscosities of suspensions with various filler volume fractions ϕ at temperatures of 15 °C (Δ), 25 °C (\circ) and 35 °C (\times). (b) Same as (a) but stress values for all suspensions at a given temperature have been shifted by a factor $a_\sigma(T)$ (see (d)) to collapse all data onto the curves obtained at 25 °C. (c) Same as (a) but with the constraint-model, Equation 2 and Equation 3, fitted to data at each temperature (full line 15 °C; dashed line 25 °C; dotted line 35 °C) using $\beta = 0.39$, $\phi_{\text{rlp}} = 0.31$, $\phi_{\text{alp}} = 0.18$. (d) Values of $\sigma_a(T)$ used in the constraint-model fits in (c). Shaded (grey) area in (a)-(c) marks the region of stresses in which sample fracture was observed.

tic adhesive stress $\sigma_a = \sigma_a(T)$ that decreases with temperature. Further investigations are required to determine the underlying cause of this observation. The adhesive stress should be related to a critical torque $\sigma_a \propto M^*/R^3$ to peel apart adhesive contacts between particles with a mean size R^{24} , so that the temperature-dependence we observe should also manifest in single-particle measurement of the contact tribology⁵⁸.

Finally, and more generally, that the adhesive constraint model²⁵ can give a credible account of data for PMMA spheres in oil²⁴, cornstarch in oil²⁵, calcite in glycerol-water²⁶ and molten chocolate (= sugar grains in oil)³⁸, and now, plate-like graphite in oil, suggests that the micro-physical basis of this model may be sound. In particular, our finding that $\phi_{\text{alp}} \approx 0.18$ is significantly higher than what one might expect from contact percolation alone in flake-like particles provides support for the suggestion^{25,26} that yielding behaviour is due to the combined action of adhesive contacts stabil-

ising frictional force chains. Our work therefore illustrates the advantage of fitting data using such a model compared to a purely phenomenological equation such as the Herschel-Bulkley model. A physics-based model permits inference about microscale mechanisms, such as temperature-dependent adhesive contacts, which are susceptible to further experimental testing.

ACKNOWLEDGMENTS

This work was financially supported by Advent Technologies A/S and a grant from the Industrial PhD programme, Innovation Fund Denmark, project 8053-00063B.

DATA AVAILABILITY STATEMENT

The data that support the findings of this study are available from the corresponding author upon reasonable request.

- ¹J. Zhang, Y.-W. Zou, and J. He, "Influence of graphite particle size and its shape on performance of carbon composite bipolar plate," *J. Zhejiang Univ. Sci.* **6A**, 1080–1083 (2005).
- ²A. Naz, A. Kausar, M. Siddiq, and M. A. Choudhary, "Comparative Review on Structure, Properties, Fabrication Techniques, and Relevance of Polymer Nanocomposites Reinforced with Carbon Nanotube and Graphite Fillers," *Plast. Technol. Eng.* **55**, 171–198 (2016).
- ³K. Yao, D. L. Adams, A. Hao, J. P. Zheng, and R. Liang, "Highly conductive, strong, thin and lightweight graphite-phenolic resin composite for bipolar plates in proton exchange membrane fuel cells," *ECS Trans.* **77**, 1303 (2017).
- ⁴R. Sengupta, M. Bhattacharya, S. Bandyopadhyay, and A. K. Bhowmick, "A review on the mechanical and electrical properties of graphite and modified graphite reinforced polymer composites," *Prog. Polym. Sci.* **36**, 638–670 (2011).
- ⁵B. K. Kakati, V. K. Yamsani, K. S. Dhathathreyan, D. Sathiyamoorthy, and A. Verma, "The electrical conductivity of a composite bipolar plate for fuel cell applications," *Carbon* **47**, 2413–2418 (2009).
- ⁶C. M. F. Calixto, R. K. Mendes, A. C. de Oliveira, L. A. Ramos, P. Cervini, and E. T. G. Cavalheiro, "Development of graphite-polymer composites as electrode materials," *Mater. Res.* **10**, 109–114 (2007).
- ⁷S. Lim, S. Kim, K. H. Ahn, and S. J. Lee, "Stress development of Li-ion battery anode slurries during the drying process," *Ind. Eng. Chem. Res.* **54**, 6146–6155 (2015).
- ⁸J. H. Lee, Y. K. Jang, C. E. Hong, N. H. Kim, P. Li, and H. K. Lee, "Effect of carbon fillers on properties of polymer composite bipolar plates of fuel cells," *J. Power Sources* **193**, 523–529 (2009).
- ⁹J. A. King, F. A. Morrison, J. M. Keith, M. G. Miller, R. C. Smith, M. Cruz, A. M. Neuhalfen, and R. L. Barton, "Electrical conductivity and rheology of carbon-filled liquid crystal polymer composites," *J. Appl. Polym. Sci.* **101**, 2680–2688 (2006).
- ¹⁰J. A. King, T. M. Tambling, F. A. Morrison, J. M. Keith, A. J. Cole, and R. M. Pagel, "Effects of carbon fillers on the rheology of highly filled liquid-crystal polymer based resins," *J. Appl. Polym. Sci.* **108**, 1646–1656 (2008).
- ¹¹M. P. da Silva, S. N. Cavalcanti, A. M. Alves, D. M. G. Freitas, P. Agrawal, E. O. Vilar, and T. J. A. de Melo, "Evaluation of the rheological and electrical percolation of high-density polyethylene/carbon black composites using mathematical models," *Polym. Eng. Sci.* **61**, 2105–2116 (2021).
- ¹²T.-S. Wei, F. Y. Fan, A. H. Helal, K. C. Smith, G. H. McKinley, Y.-M. Chiang, and J. A. Lewis, "Biphasic electrode suspensions for Li-ion semi-solid flow cells with high energy density, fast charge transport, and low-dissipation flow," *Adv. Energy Mater.* **5**, 1500535 (2015).
- ¹³M. Doi and S. F. Edwards, *The Theory of Polymer Dynamics*, International series of monographs on physics (Clarendon Press, 1988).
- ¹⁴T. C. B. McLeish, "Tube theory of entangled polymer dynamics," *Adv. Phys.* **51**, 1379–1527 (2002), <https://doi.org/10.1080/00018730210153216>.
- ¹⁵L. Ma, J. Wang, A. M. Marconnet, A. C. Barbati, G. H. McKinley, W. Liu, and G. Chen, "Viscosity and thermal conductivity of stable graphite suspensions near percolation," *Nano Lett.* **15**, 127–133 (2015).
- ¹⁶R. Zheng, J. Gao, J. Wang, S.-P. Feng, H. Ohtani, J. Wang, and G. Chen, "Thermal percolation in stable graphite suspensions," *Nano Lett.* **12**, 188–192 (2012).
- ¹⁷J. F. Morris, "Shear thickening of concentrated suspensions: Recent developments and relation to other phenomena," *Ann. Rev. Fluid Mech.* **52**, 121–144 (2020), <https://doi.org/10.1146/annurev-fluid-010816-060128>.
- ¹⁸N. M. James, E. Han, R. A. L. de la Cruz, J. Jureller, and H. M. Jaeger, "Interparticle hydrogen bonding can elicit shear jamming in dense suspensions," *Nature Mat.* **17**, 965–970 (2018).
- ¹⁹R. Mari, R. Seto, J. F. Morris, and M. M. Denn, "Shear thickening, frictionless and frictional rheologies in non-brownian suspensions," *J. Rheol.* **58**, 1693–1724 (2014), <https://doi.org/10.1122/1.4890747>.
- ²⁰M. Wyart and M. E. Cates, "Discontinuous shear thickening without inertia in dense non-Brownian suspensions," *Phys. Rev. Lett.* **112**, 098302 (2014).
- ²¹B. M. Guy, M. Hermes, and W. C. K. Poon, "Towards a unified description of the rheology of hard particle suspensions," *Phys. Rev. Lett.* **115**, 088304 (2015).
- ²²J. R. Royer, D. L. Blair, and S. D. Hudson, "A rheological signature of frictional interactions in shear thickening suspensions," *Phys. Rev. Lett.* **116** (2016).
- ²³M. Hermes, B. M. Guy, W. C. K. Poon, G. Poy, M. E. Cates, and M. Wyart, "Unsteady flow and particle migration in dense, non-brownian suspensions," *J. Rheol.* **60**, 905–916 (2016).
- ²⁴B. M. Guy, J. A. Richards, D. J. M. Hodgson, E. Blanco, and W. C. K. Poon, "Constraint-based approach to granular dispersion rheology," *Phys. Rev. Lett.* **121**, 128001 (2018).
- ²⁵J. A. Richards, B. M. Guy, E. Blanco, M. Hermes, G. Poy, and W. C. K. Poon, "The role of friction in the yielding of adhesive non-Brownian suspensions," *J. Rheol.* **64**, 405–412 (2020).
- ²⁶J. A. Richards, R. E. O'Neill, and W. C. K. Poon, "Turning a yield-stress calcite suspension into a shear-thickening one by tuning inter-particle friction," *Rheol. Acta* **60**, 97–106 (2021).
- ²⁷Y. Jiang, S. Makino, J. R. Royer, and W. C. K. Poon, "Flow-switched bistability in a colloidal gel with non-brownian grains," *Phys. Rev. Lett.* **128** (2022).
- ²⁸C. Ancey, P. Coussot, and P. Evesque, "A theoretical framework for granular suspensions in a steady simple shear flow," *J. Rheol.* **43**, 1673 (1999).
- ²⁹S. Mueller, E. W. Llewellyn, and H. M. Mader, "The rheology of suspensions of solid particles," *Proc. R. Soc. A* **466**, 1201–1228 (2010).
- ³⁰S. H. Maron and P. E. Pierce, "Application of Ree-Eyring generalized flow theory to suspensions of spherical particles," *J. Colloid Sci.* **11**, 80–95 (1956).
- ³¹I. M. Krieger and T. J. Dougherty, "A mechanism for non-Newtonian flow in suspensions of rigid spheres," *J. Rheol.* **3**, 137 (1959).
- ³²Note that in the Krieger-Dougherty equation the exponent was chosen as $l = [\eta]\phi_f$, with $[\eta]$ the intrinsic viscosity, to give the correct first-order term for a Taylor expansion in the dilute limit. While this happens to give a reasonable numerical value for l for spherical particles, there is no fundamental physical reason for the intrinsic viscosity, describing single-particle hydrodynamic contributions, to control the divergence near jamming.
- ³³C. R. Wildemuth and M. C. Williams, "Viscosity of suspensions modeled with a shear-dependent maximum packing fraction," *Rheol. Acta* **23**, 627–635 (1984).
- ³⁴J. J. Stickel and R. L. Powell, "Fluid mechanics and rheology of dense suspensions," *Annu. Rev. Fluid Mech.* **37**, 129–149 (2005).
- ³⁵L. Silbert, "Jamming of frictional spheres and random loose packing," *Soft Matter* **6**, 2918–2924 (2010).
- ³⁶W. Liu, Y. Jin, S. Chen, H. A. Makse, and S. Li, "Equation of state for random sphere packings with arbitrary adhesion and friction," *Soft Matter* **13**, 421–427 (2017).
- ³⁷In such a system, shear thickening is not observed; in a loose sense, the ever presence of friction means that flow is always frictional, so that the system is 'always shear thickened'.
- ³⁸F. Blanc, E. D'Ambrosio, L. Lobry, F. Peters, and E. Lemaire, "Universal scaling law in frictional non-Brownian suspensions," *Phys. Rev. Fluids* **3**, 114303 (2018).
- ³⁹S. Torquato and F. H. Stillinger, "Jammed hard-particle packings: From Kepler to Bernal and beyond," *Rev. Mod. Phys.* **82**, 2633–2672 (2010).
- ⁴⁰R. S. Farr and R. D. Groot, "Close packing density of polydisperse hard spheres," *J. Chem. Phys.* **131**, 244104 (2009).
- ⁴¹F. Khalkhal and P. J. Carreau, "Scaling behavior of the elastic properties of non-dilute MWCNT-epoxy suspensions," *Rheol. Acta* **50**, 717–728 (2011).
- ⁴²T. Ebeling, M. Paillet, R. Borsali, O. Diat, A. Dufresne, J.-Y. Cavallé, and H. Chanzy, "Shear-Induced Orientation Phenomena in Suspensions of Cellulose Microcrystals, Revealed by Small Angle X-ray Scattering," *Langmuir* **15**, 6123–6126 (1999).
- ⁴³R. Zouari, T. Domenech, B. Vergnes, and E. Peuvrel-Disdier, "Time evolution of the structure of organoclay/polypropylene nanocomposites and application of the time-temperature superposition principle," *J. Rheol.* **56**, 725 (2012).
- ⁴⁴A. Papadopolou, J. J. Gillissen, H. J. Wilson, M. K. Tiwari, and S. Balabani, "On the shear thinning of non-Brownian suspensions: Friction or

- adhesion?" J. Nonnewton Fluid Mech. **281**, 104298 (2020).
- ⁴⁵H. Watanabe, M.-L. Yao, A. Yamagishi, K. Osaki, T. Shitata, H. Niwa, and Y. Morishima, "Nonlinear rheological behavior of a concentrated spherical silica suspension," Rheol. Acta **35**, 433–445 (1996).
- ⁴⁶M. Schmidt, "Rheological properties of suspensions with spherical particles in shear and elongational flows," Appl. Rheol. **11**, 220–227 (2001).
- ⁴⁷S. Constanzo, V. Vanzanella, B. D. Vito, and N. Grizzuti, "Viscoelastic properties of suspensions of noncolloidal hard spheres in a molten polymer," Phys. Fluids **31**, 073105 (2019).
- ⁴⁸C. Mobuchon, P. J. Carreau, M.-C. Heuzey, and M. Sepehr, "Shear and extensional properties of short glass fiber reinforced polypropylene," Polym. Compos. **26**, 247–264 (2005).
- ⁴⁹M. M. Mowes, F. Fleck, and M. Kluppel, "Effect of filler surface activity and morphology on mechanical and dielectric properties of NBR/graphene nanocomposites," Rubber Chem. Technol. **87**, 70–85 (2014).
- ⁵⁰S. Abbasi, P. J. Carreau, A. Derdouri, and M. Moan, "Rheological properties and percolation in suspensions of multiwalled carbon nanotubes in polycarbonate," Rheol. Acta. **48**, 943–959 (2009).
- ⁵¹V. W. Herschel and R. Bulkley, "Konsistenzmessungen von Gummi-Benzollösungen," Kolloid-Z **39**, 291–300 (1926).
- ⁵²D. M. Kalyon, "Factors affecting the rheology and processability of highly filled suspensions," Annu. Rev. Chem. Biomol. Eng. **5**, 229–254 (2014).
- ⁵³D. Bonn, M. M. Denn, L. Berthier, T. Divoux, and S. Manneville, "Yield stress materials in soft condensed matter," Rev. Mod. Phys. **89**, 035005 (2017).
- ⁵⁴H. A. Barnes, "The yield stress - a review or 'παντα ρει' - everything flows," J. Non-Newtonian Fluid Mech. **81**, 133–178 (1999).
- ⁵⁵S. Gallier, E. Lemaire, F. Peters, and L. Lobry, "Percolation in suspensions and de Gennes conjectures," Phys. Rev. E. **92**, 020301 (2015).
- ⁵⁶R. A. Antunes, M. C. L. de Oliveira, G. Ett, and V. Ett, "Carbon materials in composite bipolar plates for polymer electrolyte membrane fuel cells: A review of the main challenges to improve electrical performance," J. Power Sources **196**, 2945–2961 (2011).
- ⁵⁷J. N. Israelachvili, *Intermolecular and surface forces*, 2nd ed. (Academic Press, London, 1992).
- ⁵⁸L.-O. Heim, J. Blum, M. Preuss, and H.-J. Butt, "Adhesion and friction forces between spherical micrometer-sized particles," Phys. Rev. Lett. **83**, 3328–3331 (1999).